Combustion and Flame 157 (2010) 1179–1193

Contents lists available at ScienceDirect

Combustion and Flame

journal homepage: www.elsevier.com/locate/combustflame

Effects of primary breakup modeling on spray and combustion characteristics of compression ignition engines

S. Som, S.K. Aggarwal *

Department of Mechanical and Industrial Engineering, University of Illinois at Chicago, Chicago, IL 60607, USA

ARTICLE INFO

Article history:
Received 29 August 2009
Received in revised form 22 October 2009
Accepted 22 February 2010
Available online 19 March 2010

Keywords:
Primary breakup
Diesel combustion
Kelvin–Helmholtz model
Cavitation
Turbulence
X-ray radiography
Flame lift-off
Liquid length

ABSTRACT

Injector flow dynamics and primary breakup processes are known to play a pivotal role in determining combustion and emissions in diesel engines. In the present study, we examine the effects of primary breakup modeling on the spray and combustion characteristics under diesel engine conditions. The commonly used KH model, which considers the aerodynamically induced breakup based on the Kelvin–Helmholtz instability, is modified to include the effects of cavitation and turbulence generated inside the injector. The KH model and the new (KH-ACT) model are extensively evaluated by performing 3-D time-dependent simulations with detailed chemistry under diesel engine conditions. Results indicate that the inclusion of cavitation and turbulence enhances primary breakup, leading to smaller droplet sizes, decrease in liquid penetration, and increase in the radial dispersion of spray. Predictions are compared with measurements for non-evaporating and evaporating sprays, as well as with flame measurements. While both the models are able to reproduce the experimentally observed global spray and combustion characteristics, predictions using the KH-ACT model exhibit closer agreement with measurements in terms of liquid penetration, cone angle, spray axial velocity, and liquid mass distribution for non-evaporating sprays. Similarly, the KH-ACT model leads to better agreement with respect to the liquid length and vapor penetration distance for evaporating sprays, and with respect to the flame lift-off location for combusting sprays. The improved agreement is attributed to the ability of the new model to account for the effects of turbulence and cavitation generated inside the injector, which enhance the primary breakup. Results further indicate that the combustion under diesel engine conditions is characterized by a double-flame structure with a rich premixed reaction zone near the flame stabilization region and a non-premixed reaction zone further downstream. This flame structure is consistent with the Dec's model for diesel engine combustion (Dec, 1997) [1], and well captured by a newly developed flame index based on the scalar product of CO and O_2 mass fraction gradients.

1. Introduction

The diesel engine has been the preferred power train for heavy-duty applications due to high energy density and efficiency. Moreover, there has been noticeable reduction in pollutants and noise emissions as a result of many innovations, especially in direct injection systems combined with turbo charging. However, engine manufacturers continue to face new challenges to improve engine efficiency and meet increasingly stringent emission regulations with respect to NO_x and particulate matter. For instance, the US EPA's current requirements for heavy duty truck engines manufactured after 1st January 2008 are set at 0.01 g/bhp-h for particulates and 0.2 g/bhp-h for NO_x, both an order of magnitude lower than those a decade ago. This provides a clear motivation for engine manufacturers to make enhancements in fuel injection system and combustion processes, based on fundamental understanding, and further reduce engine's raw emissions and improve fuel consumption.

In a diesel engine the liquid fuel is injected into the combustion chamber near the end of the compression stroke. Following injection, the fuel undergoes atomization and vaporization processes, followed by fuel–air mixing, ignition, and establishment of a lifted flame in the chamber. The dominant combustion processes associated with this flame are illustrated in Fig. 1, which is based on experimentally obtained laser sheet images of diesel combustion [2]. The figure shows a cold fuel jet (dark brown[1] region) and a fuel vapor rich region (light brown region) preceding a fuel-rich premixed flame (represented by the thin blue region), and a diffusion

* Corresponding author. Address: University of Illinois at Chicago, Department of Mechanical & Industrial Engineering, 842 West Taylor Street, Chicago, IL 60607-7022, USA. Fax: +1 312 413 0441.
E-mail address: ska@uic.edu (S.K. Aggarwal).

[1] For interpretation of color in Figs. 1, 3–17 the reader is referred to the web version of this article.

0010-2180/$ - see front matter © 2010 The Combustion Institute. Published by Elsevier Inc. All rights reserved.
doi:10.1016/j.combustflame.2010.02.018

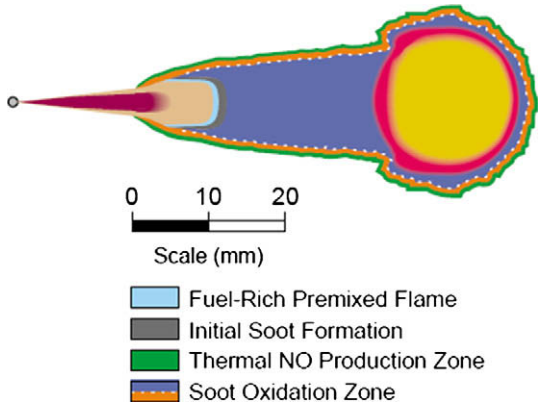

Fig. 1. Schematic of "conceptual" combustion model of Dec [1].

flame that surrounds the burning plume. Thus the combustion is characterized by a partially premixed or dual flame mode involving a rich premixed zone and a diffusion reaction zone. The dark blue region between these two reaction zones contains the products of incomplete oxidation due to rich combustion, which behave as intermediate fuels (CO, H_2, C_2H_2, etc.) and subsequently burn in the diffusion reaction zone. This region also represents the dominant soot initiation and formation zone, while most of the NO_x formation occurs in the diffusion flame, since it has the highest temperatures. The detailed structure of this dual flame and its emission characteristics strongly depend upon the location at which the flame is stabilized, i.e., the flame lift-off length, defined as the farthest upstream location of combustion on the spray axis. Thus the combustion and emission characteristics of a diesel engine are strongly coupled with the flame lift-off behavior, as demonstrated by several previous studies [1,3–6]. Since the flame lift-off characteristics are largely determined by the fuel atomization, vaporization, subsequent fuel–air mixing, and air entrainment upstream of the lift-off location, it is clear that these processes play a critical role in determining the engine combustion and emission characteristics.

The coupling between the spray and fuel–air mixing processes and the engine combustion and emissions has been investigated in previous studies [3–5,7–11]. Reitz and co-workers [9–11] performed experiments and simulations using KIVA, and examined the effects of injection, atomization and spray characteristics on the diesel engine combustion and emissions. Arcoumanis et al. [8] and Arcoumanis and Gavaises [12] numerically investigated the effects of nozzle flow and injection processes on the structure of diesel sprays. Siebers and co-workers [3–5] reported a series of experimental studies using an optically accessible, constant-volume vessel under diesel engine conditions, and investigated the effects of various injection and ambient parameters, including nozzle orifice diameter, injection pressure, ambient temperature, and density, on the combustion and emission characteristics. The effects were characterized in terms of the liquid length (L_l) and flame lift-off length (L_f). The liquid length is defined as the farthest penetration of liquid fuel in terms of the axial location [6], and is established where total fuel evaporation rate equals the injection rate. It represents a global parameter for characterizing the atomization and vaporization behavior, whereas the lift-off length is used to represent the combustion behavior. Siebers and Higgins [4] also examined interactions between these two parameters. For instance, $L_f > L_l$ implies that fuel evaporation is completed before combustion process begins, and the flame is established in a relatively rich mixture. On the other hand, for $L_f < L_l$, there is two-way coupling between combustion and spray processes, with the combustion process enhancing fuel evaporation and the relatively cooler spray decreasing the flame temperature.

The fuel injection and atomization processes are extremely complex involving transient two-phase, turbulent flows at high pressures, with a wide range of temporal and spatial scales. Consequently, the theoretical and computational studies of these flows have been very challenging. Various approaches used to model these flows can be broadly grouped into two categories. One approach follows an Eulerian–Lagrangian methodology [13], whereby the gas-phase equations are solved using Reynolds Averaged Navier Stokes (RANS) or Large Eddy Simulation (LES) methods, while the dispersed phase is solved using a Lagrangian formulation, tracking individual droplet parcels. Appropriate algorithms are employed to interpolate the gas-phase properties at the Lagrangian locations, and to distribute the interphase source terms at the Eulerian grid. One limitation of this approach is the insufficient grid resolution in the near injector region and the grid-independence of simulations, due to the basic assumption of Eulerian cell volume being sufficiently larger than the dispersed phase volume within the cell [14]. The second approach follows the Eulerian–Eulerian two-fluid methodology [15], treating different size classes of droplets as separate and inter-penetrating phases and solving conservation equations for each one of them. A major disadvantage of this approach is the excessive computational effort required as the droplet size distribution becomes wider. Some recent studies [11,16] have employed a hybrid approach, using an Eulerian method in the dense spray region, and switching to a Lagrangian method in the dilute region. It is important to note that for any of these approaches, the accuracy of simulations critically depends upon the sub-models used to represent the various dispersed phase processes, such as atomization, droplet collision, deformation, and vaporization. In particular, the modeling of atomization, especially in the near nozzle region, has been shown to be pivotal in determining the spray and combustion characteristics in diesel engines [8,11,12,17,18]. A realistic atomization model in the primary breakup region should include the essential physics associated with the two-phase flow both inside and outside the injector.

While there have been extensive studies of the primary and secondary atomization phenomena, fundamental processes associated with these phenomena are still not well understood. The liquid jet breakup is known to be caused by the Kelvin–Helmholtz (KH) and Rayleigh Taylor (RT) instabilities at the interface of the two fluids. The KH instability is due to high shear at the interface, while the RT instability is related to density difference between the two fluids. Accordingly, the most commonly used atomization models, namely the KH and RT models, are based on a linear analysis of these instabilities [19–21]. The literature review indicates that the Eulerian–Lagrangian approach using the KH–RT atomization models has been widely employed for diesel engine simulations. Most CFD-based engine simulation codes employ this methodology, using KH model for the primary breakup and a combination of KH–RT models for the secondary breakup. This approach has been found to be computationally efficient and reproduce the global spray behavior reasonably well. However, several studies have shown that fuel atomization in the region close to the injector nozzle is also strongly influenced by cavitation and turbulence in the liquid jet [12,22]. The cavitation structures developed inside the nozzle orifice can reach the exit, implode, and cause jet integration. Similarly turbulent eddies emerging from the nozzle can cause further jet disintegration. While the effects of cavitation and turbulence on the primary breakup are well established, most of the atomization models used in CFD-based engine simulations only consider aerodynamic jet breakup based on the KH instability.

The present study aims to investigate the effects of modeling the primary breakup processes on the spray and combustion characteristics under diesel engine conditions. In our previous study [23,24], the KH model was modified to include the effects of cavi-

tation and turbulence on primary atomization, and tested using the X-ray radiography data in the near nozzle region. In the present study, this improved primary breakup model is used to examine the effects of primary breakup on the spray and combustion characteristics. Since the specification of cavitation and turbulence at the injector exit requires information about the inner nozzle flow, the primary breakup model is quasi-dynamically linked to the inner nozzle flow simulations. The KH-ACT model is comprehensively tested using the spray vaporization and combustion data reported by Siebers and co-workers [3–5]. The model is then used to examine the effects of cavitation, and turbulence on the spray and combustion characteristics under diesel engine conditions. Simulations are performed using the CFD code "CONVERGE", based on the Eulerian–Lagrangian approach [25–28].

The effects of cavitation and turbulence on primary atomization have been investigated in some previous studies. Arcoumanis and Gavaises [8] examined the effect of cavitation using a 1-D wave model for the injector flow dynamics. Huh and Gosman [29] developed a phenomenological model to consider the effects of turbulence on the jet breakup. Bianchi et al. [30] included the effects of cavitation and turbulence in the KH model. However, cavitation and turbulence levels at the nozzle exit were computed using a 1-D model and an analytical expression, respectively, while in our approach, the improved primary breakup model is quasi-dynamically linked to the inner nozzle flow simulations. As noted in the next section, there are also other differences pertaining to the implementation of turbulence and cavitation effects in the model. Berg et al. [31] examined the effects of turbulence and cavitation by dynamically coupling the inner nozzle and spray simulations. In summary, except for the study of Berg et al., the effects of cavitation, liquid-phase turbulence, and inner nozzle flow on spray and combustion characteristics have not previously been comprehensively investigated. While the above effects have been examined under some conditions, the ability to capture the spray characteristics even qualitatively with varying degree of cavitation and turbulence has not been established. This provided the major motivation for the present study.

The paper is organized as follows. First we briefly describe the physical–numerical model, including a description of the improved primary breakup (KH-ACT) model incorporating the cavitation and turbulence effects. Then we discuss results in two parts. The first part deals with the effects of primary breakup modeling on the non-evaporating spray characteristics, while the second part focuses on differences between the KH and KH-ACT models in predicting the evaporating and reacting spray characteristics under diesel engine conditions. Conclusions are presented in the last section.

2. Physical–numerical model

The physical–numerical model is based on an Eulerian–Lagrangian description of the two-phase flow. The gas-phase flow field is described using the Favre-Averaged Navier–Stokes equations in conjunction with the RNG k–ε turbulence model. The length and time scales for the spray are too small to be resolved computationally, necessitating the use of sub-grid scale models to describe the spray physics. The spray is represented by a stochastic system of a discrete number of parcels, which are tracked computationally using a Lagrangian scheme. The two-phases are coupled through the mass, momentum, and energy exchange terms, which are present in both the liquid- and gas-phase equations. The gas-phase equations are solved on a Eulerian grid using a finite volume methodology, and a semi-implicit hybrid scheme. All the transported quantities are collocated at the cell center as opposed to a staggered arrangement. The Rhie–Chow interpolation scheme was used to maintain the collocated variables and eliminate undesirable checker boarding which can arise due to a staggered approach. The pressure–velocity coupling is achieved using the Pressure Implicit with Splitting of Operators (PISOs) method. Further details can be found in Refs. [27,28].

2.1. Grid generation

Simulations are performed using a CFD code 'CONVERGE' [25–27], which employs an innovative cut-cell Cartesian method for grid generation. The grid is generated internally to the code at runtime. For non-evaporating sprays the base grid size was fixed to 4 mm. In order to resolve the flow field near the injector, a fixed grid embedding was employed with three levels of adaptive mesh refinement for the velocity field such that the minimum grid size was 0.5 mm. A cylindrical geometry of 50 mm in diameter and 200 mm in length was generated. Fig. 2 presents the adaptive mesh evolution with time for the non-evaporating spray simulations. For evaporating sprays the base grid size was fixed to 8 mm. A fixed grid embedding was employed such that the minimum grid size was 0.5 mm, and four levels of adaptive mesh refinement were employed for the velocity field. In order to match the spray chamber geometry, a cube of 108 mm was generated.

2.2. Spray and combustion models

Spray processes that were modeled include the following: jet atomization, droplet breakup, drop distortion and drag, droplet interactions in terms of collision and coalescence, turbulent dispersion, drop vaporization, and spray wall interaction. The two-phases are coupled through the exchange of mass, momentum, and energy, represented by the appropriate source terms in the gas-phase equations. Since these models are discussed elsewhere [25–27], only a brief description is provided here. However, the KH breakup

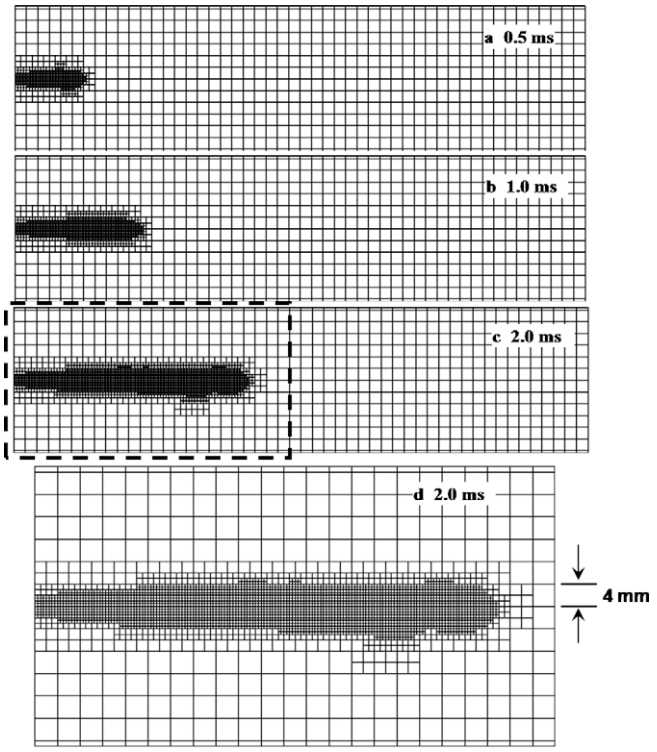

Fig. 2. Grid generated in CONVERGE at different times during the simulation for non-evaporating sprays described in Table 1. The field of view in axial and radial direction is 200 mm and 50 mm, respectively.

model, which is the primary focus of this study, is described in some detail. Droplet collisions are based on the No Time Counter (NTC) algorithm [32]. Once collision occurs, the outcomes of the collision are predicted as bouncing stretching, reflexive separation, or coalescence [33]. A single component droplet evaporation model [13] based on Frossling correlation is used. A dynamic drag model is used which accounts for the effects of drop distortion, linearly varying between the drag of a sphere and a disk [34]. Liquid–gas coupling is performed using the nearest node approach [27]. The effects of turbulence on droplet dynamics is included through a standard turbulent dispersion model [13]. Detailed kinetic modeling is performed using the SAGE chemical kinetic solver [25–27] with n-heptane mechanism developed at Chalmers University [35]. The mechanism consists of 42 species and 168 reactions for n-heptane combustion and NO_x formation, and was directly coupled with the gas phase calculations using a well-stirred reactor model.

2.3. KH model

The injection process is simulated using a blob model, which injects liquid droplet parcels with a diameter equal to an effective nozzle diameter. The KH and the KH-ACT primary breakup models are used to predict the subsequent droplet breakup. The KH model considers breakup resulting from unstable waves growing at the liquid surface. Due to the relative velocity between the gas and liquid phases, the growth of KH instabilities induces the shearing of the droplets from the liquid surface as depicted in Fig. 3a. The breakup of droplet parcels is calculated by assuming that the radius of newly formed droplets (r_{KH}) is proportional to the wavelength of the fastest growing unstable surface wave on the parent droplet i.e.,

$$r_{KH} = B_0 \Lambda_{KH} \tag{1}$$

where B_0 is a constant. Λ_{KH} is the wavelength corresponding to the KH wave with the maximum growth rate Ω_{KH} given by:

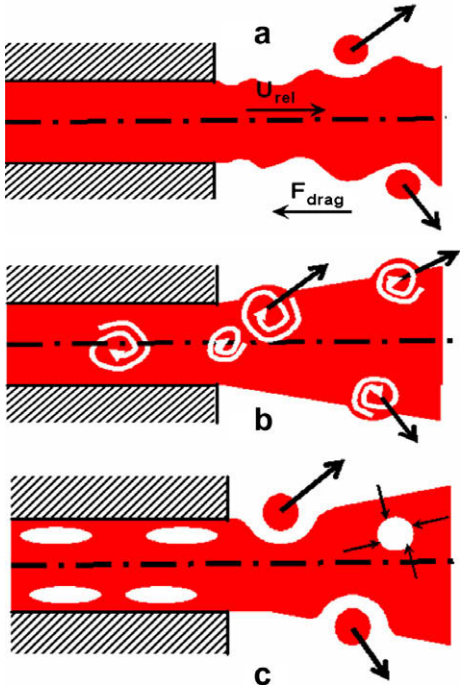

Fig. 3. Schematic representation of different primary breakup mechanisms (a) aerodynamically induced, (b) turbulence induced, and (c) cavitation induced.

$$\Omega_{KH} = \frac{0.34 + 0.38We_g^{1.5}}{(1+Z)(1+1.4T^{0.6})}\sqrt{\frac{\sigma}{\rho_l r^3}} \tag{2}$$

$$\Lambda_{KH} = \frac{9.02r\left(1+0.45\sqrt{Z}\right)(1+0.4T^{0.7})}{(1+0.865We_g^{1.67})^{0.6}} \tag{3}$$

where

$$Z(Ohnesorge\,number) = \frac{\sqrt{We_l}}{\mathrm{Re}_l} \quad We_l(Weber\,Number) = \frac{\rho_l U_r^2 r}{\sigma}$$
$$\mathrm{Re}(Reynolds\,Number) = \frac{U_\gamma r}{\nu_l} \quad T(Taylor\,Number) = Z\sqrt{We_g} \tag{4}$$
$$We_g(Weber\,Number) = \frac{\rho_g U_r^2 r}{\sigma}$$

Here σ, ρ_g, U_r, ρ_l, and ν_l are, respectively, the surface tension, gas density, relative velocity magnitude between the two-phases, liquid density, and liquid viscosity. During breakup the radius of the parent droplet parcel (r) decreases continuously according to the following equation until it reaches the stable droplet radius (r_{KH}):

$$\frac{dr}{dt} = \frac{r - r_{KH}}{\tau_{KH}}, \quad r_{KH} \le r \tag{5}$$

$$\tau_{KH}(Breakup\ time) = \frac{3.276B_1 r}{\Omega_{KH}\Lambda_{KH}} \tag{6}$$

Here B_1 is a KH model constant. Mass is accumulated from the parent droplet until the shed mass is equal to 5% of the initial parcel mass. At this time a new parcel is created with a radius given by Eq. (1). Except for the radius and velocity, the new parcel is given the same properties as the parent parcel. The new parcel is given a component of velocity randomly selected in the plane orthogonal to the direction of the parent parcel, and the momentum of the parent parcel is adjusted so that the momentum is conserved. The magnitude of the new parcel velocity is the same as that of the parent parcel. The child droplets undergo secondary breakup due to the competing effects of KH and Rayleigh Taylor [9,21] models. A breakup length [21] is employed such that the KH or KH-ACT model is employed for primary breakup in the breakup length region, whereas the KH and RT models compete to breakup the droplet outside the breakup length. The model constants used can be found in our previous studies [36].

As discussed earlier, the primary breakup in the region very close to the injector nozzle is also influenced by cavitation and turbulence generated inside the nozzle. The improved primary breakup model incorporating these effects is described below.

2.4. Turbulence induced breakup

According to Huh and Gosman [29] the turbulent fluctuations in the jet are responsible for the initial perturbations on the jet surface. These waves grow according to KH instabilities until they breakup from the surface as depicted in Fig. 3b. The relevant length ($L_T(t)$) and time ($\tau_T(t)$) scales for turbulence induced breakup are calculated as follows:

$$L_T(t) = C_\mu\left(K(t)^{1.5}/\varepsilon(t)\right) \tag{7}$$

$$\tau_T(t) = C_\mu(K(t)/\varepsilon) \tag{8}$$

where $K(t)$ and $\varepsilon(t)$ are, respectively, the instantaneous turbulent kinetic energy and dissipation rate, and C_μ and C_ε are turbulence model constants. Assuming isotropic turbulence for the liquid phase and neglecting the diffusion, convection, and production terms in the k–ε equation, $K(t)$ and $\varepsilon(t)$ for a parcel can be estimated as:

$$K(t) = \left\{ \frac{(K_0)^{C_\varepsilon}}{K_0(1 + C_\mu - C_\mu C_\varepsilon) + \varepsilon_0 t(C_\varepsilon - 1)} \right\}^{1/(1-C_\varepsilon)} \quad (9)$$

$$\varepsilon(t) = \varepsilon_0 \left\{ \frac{K(t)}{K_0} \right\}^{C_\varepsilon} \quad (10)$$

where K_0 and ε_0 are the initial values at the nozzle exit at start of injection (SOI), determined from nozzle flow simulations [37]. The traditional approach is to determine these values using a simple force balance, not accounting for the decay in turbulence levels [30]. The approach used in this study thus provides a more accurate representation of turbulence quantities at any time step.

2.5. Cavitation induced breakup

Cavitation patterns generated inside the injector nozzle can reach the nozzle exit, and their implosion enhances jet atomization as depicted in Fig. 3c. The underlying assumption is that cavitation patterns are transported to the jet periphery by the turbulence velocity inside the liquid, and either burst at the periphery or collapse before reaching it. For both cases, a characteristics time scale is calculated, the smaller one causing breakup. Following Bianchi and Pelloni [30] and Arcoumanis and Gavaises [12], the characteristic cavitation time scale (τ_{CAV}) is calculated as:

$$\tau_{CAV} = \min(\tau_{Collapse} : \tau_{Burst}). \quad (11)$$

The bubble collapse time is calculated from Rayleigh Plesset theory [38] as the time taken for a bubble of a given radius "r" to decrease to 0:

$$\tau_{Collapse} = 0.9145 R_{CAV} \sqrt{\frac{\rho_l}{p_v}} \quad (12)$$

where, p_v is the fuel vapor pressure, ρ_l the fuel density, and R_{CAV} is the effective radius of an equivalent bubble from the nozzle calculated as:

$$R_{CAV} = r_{hole} \sqrt{(1 - C_a)} \quad (13)$$

The area reduction coefficient (C_a) is calculated from flow simulations inside the injector [37] and r_{hole} is the exit radius of the nozzle orifice. The average time required for a cavitation bubble to reach the periphery of the jet can be estimated as:

$$\tau_{Burst} = \frac{r_{hole} - R_{CAV}}{u'_{turb}} \quad (14)$$

where the turbulent velocity $u'_{turb} = \sqrt{\frac{2K(t)}{3}}$ is obtained from inner nozzle flow simulations. The length scale for the cavitation induced breakup is calculated as:

$$L_{CAV} = R_{CAV}. \quad (15)$$

2.6. Aerodynamically induced breakup model

The KH model described in the previous section is used to calculate the instantaneous length and time scales for every parcel:

$$L_{KH} = r - r_{KH} \quad (16)$$

$$\tau_{KH} = \frac{3.276 B_1 r}{\Omega_{KH} \Lambda_{KH}} \quad (17)$$

The ratio of length and time scales for each process is calculated. As seen from Eqs. (5) and (19), rate of decrease in droplet radius scales with the ratio of length to time scale. Thus the largest ratio determines the dominant breakup process.

$$\frac{L_A}{\tau_A} = \max \left\{ \frac{L_{KH}(t)}{\tau_{KH}(t)}; \frac{L_{CAV}}{\tau_{CAV}}; \frac{L_T(t)}{\tau_T(t)} \right\} \quad (18)$$

If aerodynamic-induced breakup process is dominant, then the KH model, as represented by Eq. (5), is employed for primary atomization. However, if cavitation or turbulence processes dominate then the following breakup law is used:

$$\frac{dr}{dt} = -C_{T,CAV} \frac{L_A}{\tau_A} \quad (19)$$

This new primary breakup model, which includes the effects of aerodynamics, cavitation, and turbulence, is called KH-ACT model in this paper. It should be noted that the KH-ACT model introduces only one additional constant ($C_{T,CAV}$), and its value was kept fixed for all the simulations presented in this paper. We have previously reported comprehensive validation of the KH-ACT model using measurements for non-evaporating and evaporating sprays, and for different configurations and injectors [23,28]. The same model constant was used for these validations, indicating robustness of the model. Parent parcels are subjected to primary breakup only, while child parcels are subjected to a competition between KH (or KH-ACT) and RT breakup. It is also important to note the differences between our approach and that used by Bianchi et al. [30]. First of all, the primary breakup model in the present study is quasi-dynamically linked to the inner nozzle flow simulations to provide the cavitation and turbulence levels at the nozzle exit. In the cited study, cavitation and turbulence levels at the nozzle exit were computed using simplified models. In addition, Bianchi et al. used the characteristic time scales in determining the dominant breakup mechanism, while our model considers the ratios of length and time scales. Moreover, Bianchi et al. assumed that the turbulent kinetic energy and its dissipation rate associated with a given parcel are invariant with time, whereas we consider their temporal variation using the k–ε turbulence model.

Two different injectors were considered in this study; a full-production mini-sac injector used at Argonne National Lab [39] for X-ray measurements (for non-evaporating sprays) of fuel distribution in the near nozzle region, and a common-rail injector used at Sandia National Lab [4] for evaporating and combusting spray measurements. Since sufficient information about the injector geometry, injection rate profile etc., was available for the first injector, detailed 3-D turbulent flow simulations were performed. The inner nozzle flow simulations provided the necessary boundary conditions for the primary breakup model in terms of turbulent kinetic energy, turbulence dissipation rate, and amount of cavitation [37] at the nozzle exit. Simulations were performed at different needle lift positions to obtain transient data for turbulence and cavitation parameters through the range of injection duration. Analogous to the rate of injection (ROI) profile providing information for the injected droplet parcels [37], nozzle flow simulations provided information on cavitation and turbulence levels to these parcels. Thus the changes in amount of cavitation, turbulence, discharge coefficient, and injection velocity with different nozzle geometries were computed. Consequently, compared to the KH model, which only accounts for the changes in injection velocity and discharge coefficient, the KH-ACT model is more robust. However, for the second injector, geometric details were not available, and, consequently, empirical correlations were employed to compute the turbulence and cavitation levels at the nozzle exit [30].

3. Results and discussion

In order to examine the effect of primary breakup modeling on the spray and combustion characteristics, simulations using the KH and the KH-ACT primary breakup models are compared against the measurements for non-evaporating and evaporating sprays, as well as for combusting sprays under diesel engine conditions.

Fig. 4 presents the comparison of X-ray radiography measurements with predictions using the KH and KH-ACT models for a non-evaporating spray in the near nozzle region of a full-production injector [39,40]. The experimental conditions are listed in Table 1. The comparison is shown in terms of the transverse distributions of projected mass density 0.99 ms after start of injection (SOI) at fixed axial locations for an injection pressure of 1100 bar (cf. Table 1). As discussed in Refs. [39,40], the X-ray radiography technique provides line-of-sight measurement of the liquid mass density (mass/area) in the highly dense spray region. The standard deviation in the mass density measurement was approximately 1.1 μg/mm^2, (less than 1%), with somewhat higher value in the very dense spray region [39]. These measurements represent ensemble average of 128 injections.

Simulations were performed in a 3-D geometry, and post-processed [41] to yield the projected mass density. As indicated in Fig. 4, both the models capture qualitatively the experimentally observed variation of projected mass density, which has a Gaussian distribution with the peak of this bell shape curve decreasing with the axial distance due to atomization and dispersion of resulting droplets. There are, however, quantitative differences between the two models. The KH model overpredicts the peak mass density and underpredicts spray dispersion compared to the KH-ACT model and measurements. This implies that the liquid penetration is overpredicted with the KH model. These differences can be directly attributed to the cavitation and turbulence effects, which enhance primary breakup, producing more child droplets and increasing spray dispersion for the KH-ACT model. The differences in terms of liquid penetration and spray dispersion for the two models can be seen more clearly in Fig. 5, which presents the computed spray structures in terms of the instantaneous droplet locations at 0.5 ms, 1.5 ms, and 2.5 ms after SOI. Fuel droplets are shown demarcated by their sizes. The instantaneous images clearly indicate that with the KH-ACT model, the liquid penetration is reduced while the dispersion is increased. For example, at 1.5 ms after SOI, the liquid penetration predicted with the KH model is about 15 mm higher than that obtained using the KH-ACT model. The increased dispersion leads to larger spray cone angle for the KH-ACT model; for example the predicted cone angles using the KH-ACT model and KH model are 16° and 13°, respectively. Here the cone angle is calculated by using the transverse locations at which the liquid mass density is 60% of the value at the spray axis.

Results so far have focused on the effect of primary breakup models on the near field spray behavior. The effect on the far field spray behavior is depicted in Figs. 6 and 7. Fig. 6 presents the transverse integrated mass (TIM) (Fig. 6a) and normalized axial spray velocity (Fig. 6b) vs. axial position based on X-ray measurements [39,44] and simulations at 0.99 ms after SOI for the two injection pressures. Note that spray velocity has been commonly used to characterize diesel sprays [42–44]. The TIM was obtained by integrating the projected density distribution (cf. Fig. 4) at a given time and axial location. The procedure to obtain the axial spray velocity from X-ray measurements has been described in previous studies [40,44]. In simulations, the spray velocity was computed by averaging the axial velocity on mass basis using all the droplet parcels at a given axial location. Both the predictions and measurements indicate that TIM increases up to a certain axial location and then decreases. This behavior is related to the ROI profile used and the fact that the spray broadens initially and then thins down near the head vortex, which decreases the mass per unit length in this region. The increase in TIM with axial position in the near field is

Table 1
Test conditions for X-ray radiography experiments at Argonne National Laboratory [39,40].

Parameter	Quantity
Injection system	Caterpillar HEUI 315B
Nozzle geometry	Cylindrical, non-hydroground
Number of orifices	6
Orifice diameter	169 μm with L/D = 4.412
Injection pressure (Bar)	Case 1: 1100 | Case 2: 1300
Fill gas	Nitrogen (N_2)
Chamber density (kg/m^3)	34.13
Chamber temperature (K)	298
Fuel	Viscor & cerium blend
Fuel density (kg/m^3)	865.4
Fuel injection temperature (K)	313

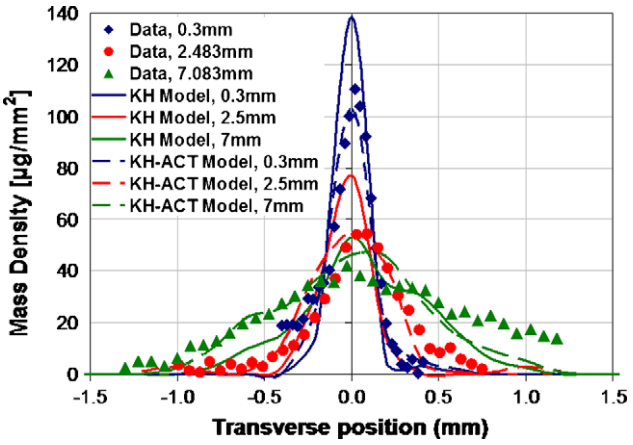

Fig. 4. Comparison of KH and KH-ACT models against X-ray data (Table 1) in terms of transverse distribution of projected liquid mass density for case 1.

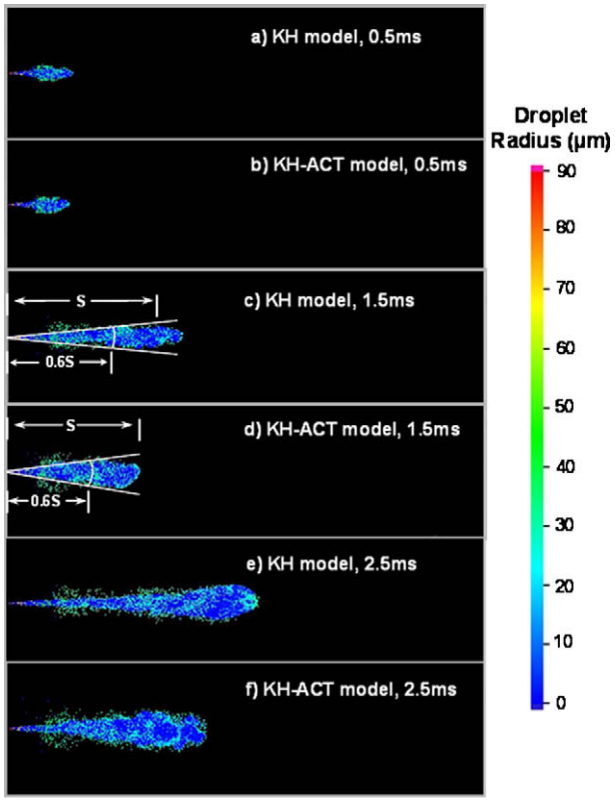

Fig. 5. Simulated spray structure at 0.5 ms for (a) KH model, (b) KH-ACT model; at 1.5 ms (c) KH model, (d) KH-ACT model; and at 2.5 ms (e) KH model, (f) KH-ACT model, for case 1 (cf. Table 1). The droplet radius scale is shown on the right. 'S' represents the peak spray tip penetration. The field of view in the axial and radial directions is 200 mm and 50 mm, respectively.

reasonably well captured by the two models. However, the KH model underpredicts TIM compared to measurements and predictions with the KH-ACT model. Moreover, the peak in TIM for the KH model occurs at a higher axial location compared to that for the KH-ACT model. These differences are related to the fact that for the same injected mass as a given instant, the liquid penetration is overpredicted with the KH model.

As indicated in Fig. 6b, the spray velocity decreases rapidly in the near field region due to high ambient density. While both the models capture this behavior, predictions using the KH-ACT model are in better agreement with measurements. The KH model overpredicts the spray velocity compared to measurements and predictions using the KH-ACT model, and the difference again is related to the reduced rate of primary atomization predicted by the KH model, which results in larger droplets with higher velocities. Note that the lack of smoothness in the predicted plots is due to the post-processing of dispersed phase properties that are based on the Lagrangian formulation.

In order to isolate the effects of cavitation and turbulence on the spray behavior, Fig. 7 presents the temporal variation of liquid penetration and Sauter Mean Diameter (SMD) computed using the two models for an injection pressure of 1100 bar. For the KH-ACT model, results are shown with the cavitation and turbulence effects included, only cavitation included, and only turbulence included. The liquid penetration has been extensively used to characterize the atomization and spray behavior in diesel engines. In our simulations, the liquid penetration is defined by the axial location which encompasses 97% of the injected fuel mass. Results in Fig. 7 indicate that the liquid penetration is strongly influenced by turbulence and cavitation generated inside the nozzle, both of which enhance the rate of primary breakup, resulting in more child parcels and thus smaller SMD, as indicated in Fig. 7b. At 3 ms from SOI, the difference between the penetration lengths predicted by the KH and KH-ACT models is as much as 20 mm. This also implies that with the KH-ACT model, the effect of ambient gas density on droplet deceleration becomes more pronounced. Moreover, for the conditions investigated, turbulence has a greater influence on primary breakup, and on liquid penetration, compared to cavitation. This is simply due to the fact that for the present conditions, the amount of cavitation generated inside the nozzle was relatively small [37]. It is also interesting to note that liquid penetration during the very early time period ($t \leqslant 0.15$ ms) is insensitive to the breakup model. This implies that the initial penetration mostly

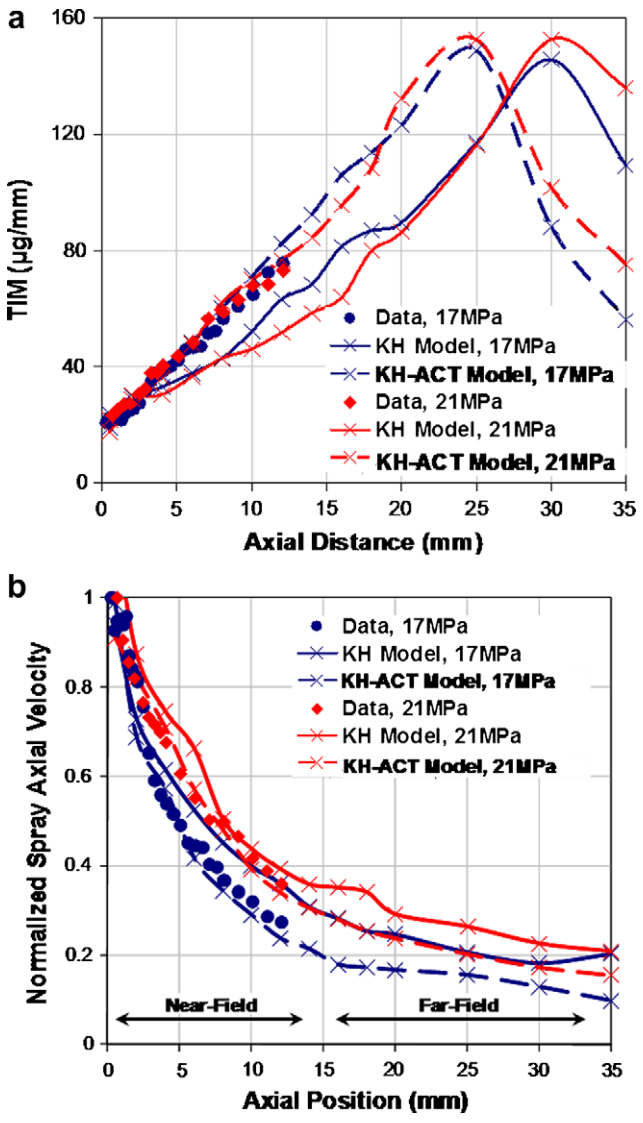

Fig. 6. Comparison of KH and KH-ACT models against the X-ray data (Table 1) in terms of (a) transverse integrated mass (TIM) vs. axial position and (b) normalized spray axial velocity vs. axial position, at 0.99 ms after SOI for cases 1 and 2.

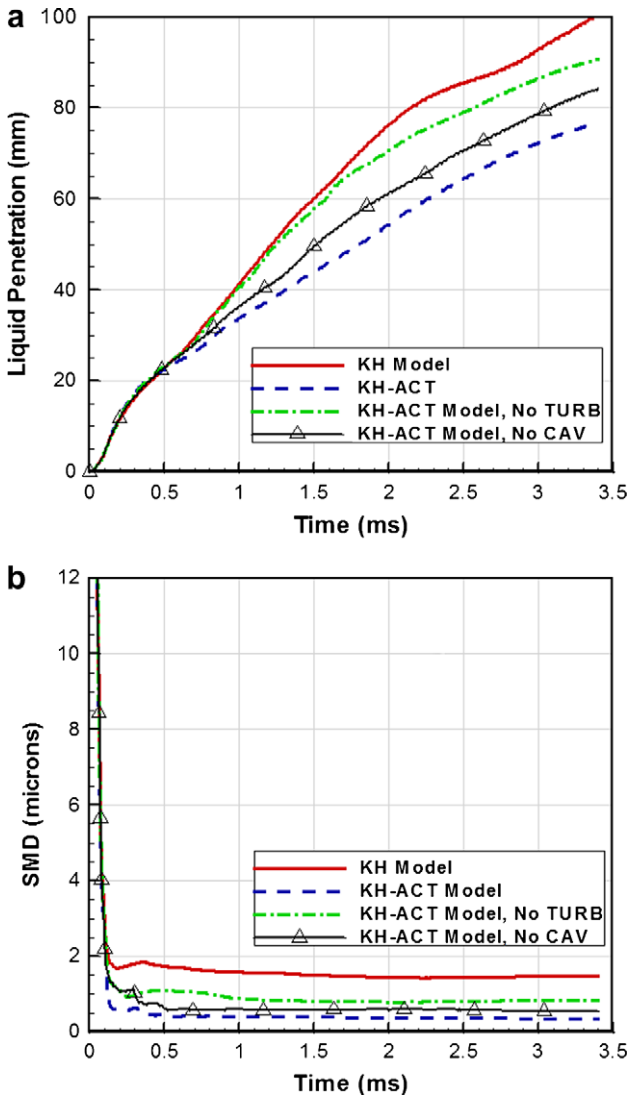

Fig. 7. Effect of different primary breakup models on (a) spray penetration and (b) Sauter Mean Diameter for the complete injection duration for case 1 (cf. Table 1).

depends on the ROI profile, and ambient gas effects become important further downstream [23,39]. Another important aspect concerns as to how far downstream the effect of cavitation and turbulence on the primary breakup lasts. Based on present results, these effects seem to be important up to about 10 mm, i.e., about 60 nozzle diameters. Further downstream, the primary breakup process is dominated by the aerodynamic or KH instability mechanism.

4. Effect of primary breakup model on evaporating spray characteristics

The effect of primary breakup modeling for evaporating sprays is examined by comparing simulations with the measurements of Naber and Siebers [3] and Siebers [6] in a constant volume combustor. The data were reported in terms of liquid length and vapor penetration distance for a range of parameters, including injection pressure, nozzle diameter, fuel temperature, ambient density and temperature. The experimental conditions are listed in Table 2. Under evaporating conditions, the liquid length is defined as the maximum liquid penetration distance. It represents an important spray characteristic since over- penetration can result in impingement on combustion chamber walls and pistons, with associated increase in engine raw emissions, while under-penetration results in poor air utilization. Similarly, vapor penetration is an important parameter in representing evaporating spray characteristic, as it defines the extent of fuel vapor penetration and thus the amount of fuel air mixing. In the simulations, the vapor penetration was defined as the distance between nozzle tip and the location of 5% fuel vapor contour at the spray tip.

Fig. 8 presents the comparison of KH and KH-ACT model against experimental data in terms of the terms of liquid length and vapor penetration distance. The comparison of experimental images of the spray with the predicted snapshots at different ambient densities is shown in Fig. 9. The orifice diameter, injection pressure, and fuel temperature are 246 μm, 142 MPa, and 438 K, respectively. As indicated in Fig. 8a, an increase in ambient temperature at a fixed density causes a decrease in liquid length, which is due to the increased vaporization rate, which decreases the droplet size, and thus the liquid length. Similarly, the vapor penetration distance decreases with the increase in ambient density, as shown in Fig. 8b. This is mainly due to the decrease in liquid length at higher ambient density. This overall behavior is fairly well captured by both the models. The predictions using KH-ACT model show somewhat better agreement with measurements compared to those using the KH model. The liquid length as well as vapor penetration length predicted by the KH-ACT model are lower than those predicted by the KH model, and this can be attributed to the enhanced primary atomization rate which decreases the liquid penetration and droplet size for the KH-ACT model, as discussed earlier. It is also interesting to note that differences between the KH and KH-ACT models are less pronounced for evaporating sprays compared to those for non-evaporating sprays. For instance, the difference in the predicted liquid penetration lengths for evaporating spray is ≈4 mm compared to ≈20 mm for non-evaporating spray (cf. Fig. 6). This is expected since the vaporization effects become more significant for evaporating sprays, especially at higher ambient temperatures. Another important observation is that the difference between simulations and predictions becomes somewhat more pronounced at high ambient densities (or pressures) and temperatures, which may be due to deficiencies in the vaporization model used in the present study.

Table 2
Test conditions for combustion experiments at Sandia National Laboratory [3–6].

Parameter	Quantity
Injection system	Detroit diesel, common rail
Nozzle geometry	Cylindrical, non-hydroground
Number of orifices	1
Orifice diameter	100–500 μm with $L/D = 4.2$
Injection pressure (Bar)	400–1800
Fill gas composition	$N_2 = 0.693$, $O_2 = 0.21$, $CO_2 = 0.061$, $H_2O = 0.036$
Chamber density (kg/m^3)	3.3–60
Chamber temperature (K)	700–1300
Fuel density (kg/m^3)	832
Fuel injection temperature (K)	400

5. Effect of primary breakup model on spray combustion characteristics

Preceding results indicated that the inclusion of cavitation and turbulence in the primary breakup model enhances the atomiza-

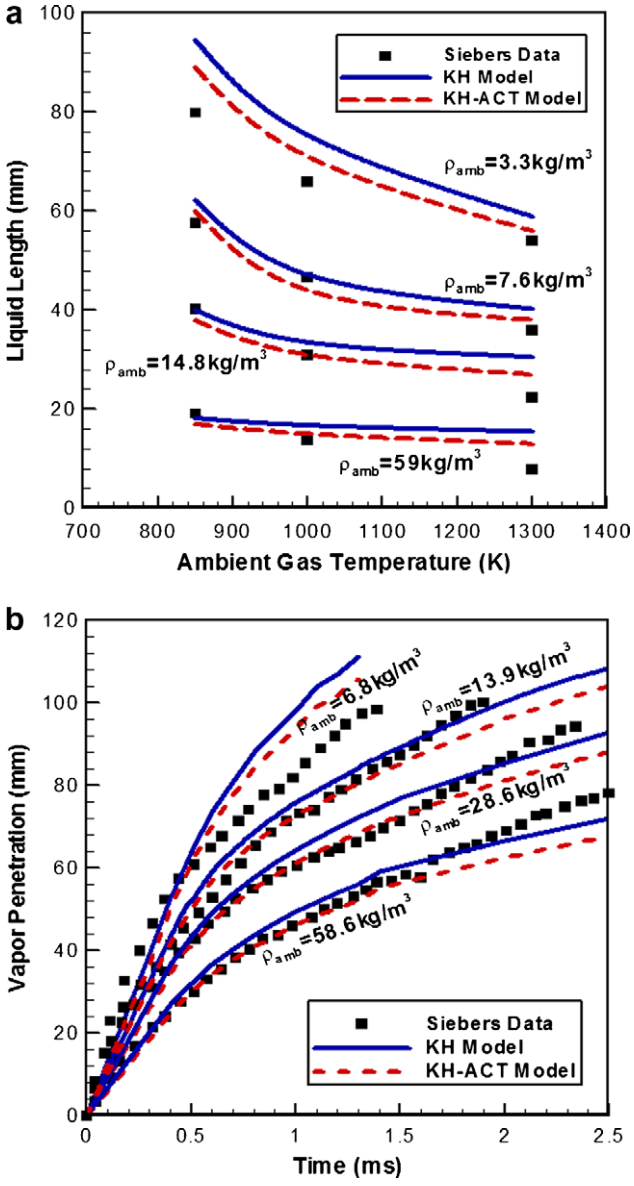

Fig. 8. Comparison of KH and KH-ACT primary breakup models against Siebers data (Table 2) in terms of (a) liquid length vs. ambient gas temperature at fixed ambient gas density and (b) vapor penetration vs. time at fixed ambient gas density.

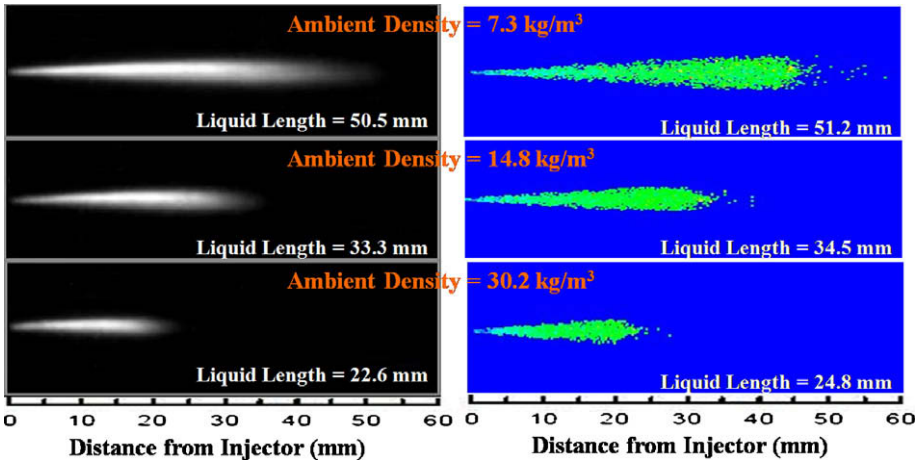

Fig. 9. Comparison of predicted spray images with Siebers measurements at different ambient gas densities. Predictions are based on the KH-ACT model.

tion rate, leading to smaller droplets, and thus smaller liquid and vapor penetration lengths. This implies that fuel air mixing, ignition, and combustion processes would also be influenced by the primary breakup model. This aspect is investigated by comparing the predictions of KH and KH-ACT models with the flame measurements of Siebers and co-workers [4,5] in a constant volume combustor under diesel engine conditions. Fig. 10 presents images from simulations using the KH-ACT breakup model at different times for the base case. The experimental conditions are listed in Table 3. Fig. 10a shows liquid fuel penetration (green color representing droplets) at 0.25 ms after SOI, while Fig. 10b shows the occurrence of ignition, indicated by the appearance of two symmetrical flame kernels near the spray at 0.625 ms after SOI. At this instant the fuel seems to have reached its maximum penetration or "liquid length" marked by the white dashed line. As the flame front develops and propagates downstream, the ignition location (base of the flame) is seen to move upstream, as indicated in Fig. 10c and d. The flame base is stabilized at about 1.5 ms after SOI, and its location is identified by the farthest upstream location of the 2200 K temperature contour on the spray axis. This location is defined as the flame stabilization location, and its distance from the nozzle exit as the flame "liftoff" length, which is marked by the white solid line.

Since Siebers and co-workers [4,5] presented experimental results in terms of the liquid length and flame lift-off length, the computational results in the present study were post-processed to obtain these two parameters under various conditions. Fig. 11 presents a comparison of the computed flame images (including lift-off locations) obtained using the KH model and KH-ACT model for the base case (cf. Table 3). The field of view is 80x 40 mm in the axial and radial directions, respectively, for images in Fig. 11a–c,

Table 3
Conditions for the base case simulations [3,4].

Parameter	Quantity
Injection pressure	142 MPa
Orifice parameters	180 μm, $L/D_0 = 4.2$
Injection duration	5 ms
Ambient gas composition	$N_2 = 0.693$, $O_2 = 0.21$, $CO_2 = 0.061$, $H_2O = 0.036$
Chamber density	14.8 kg/m3
Chamber temperature	1000 K

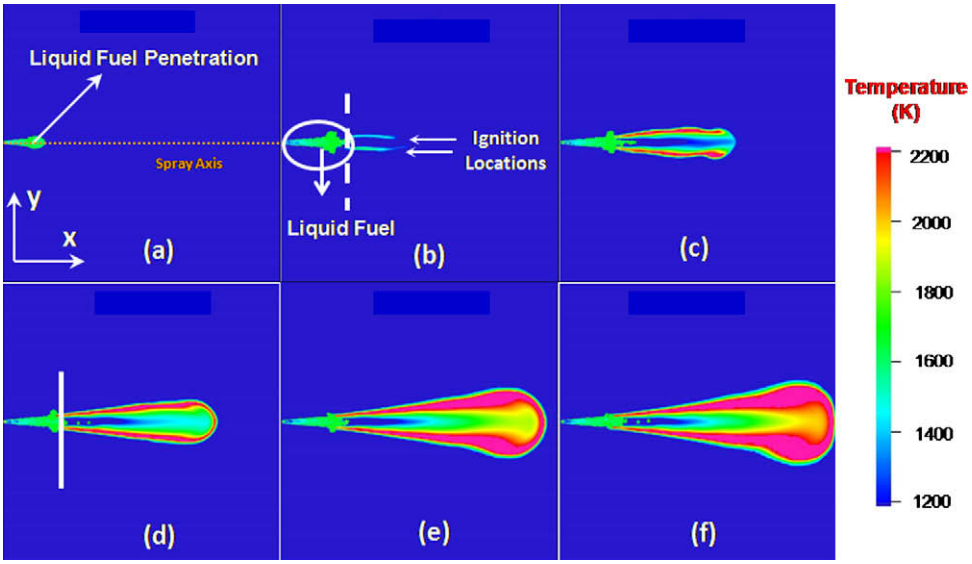

Fig. 10. Computed liquid fuel penetration and temperature contours for the base case at (a) 0.25, (b) 0.625, (c) 0.75, (d) 1.0, (e) 1.5, (f) 1.75 ms after SOI. The field of view in both axial and radial directions is 108 mm for each image.

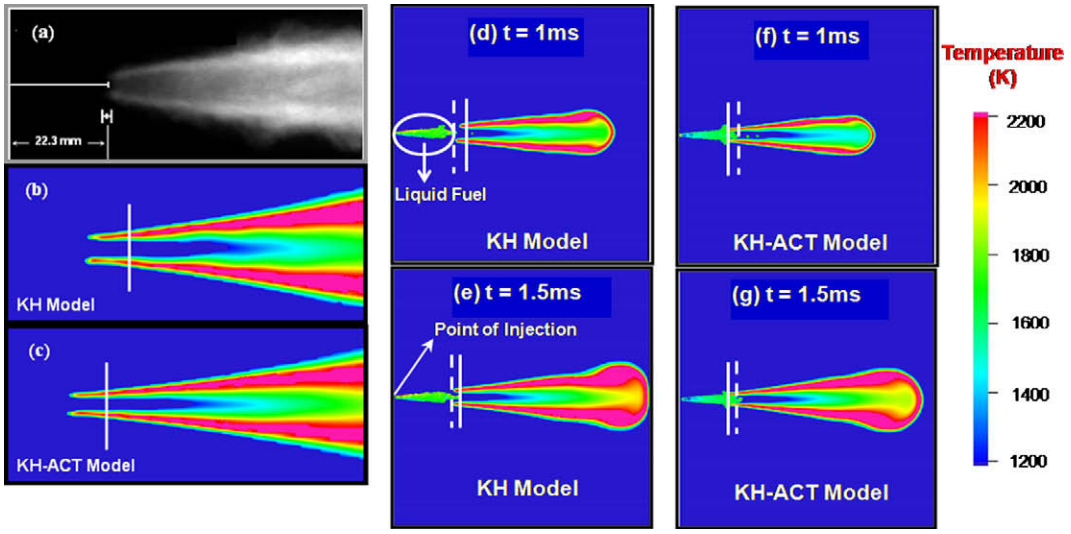

Fig. 11. (a) Measured flame image and computed flame image (in terms of temperature contours) using (b) KH model, (c) KH-ACT model under stabilized flame conditions for the base case (Table 3).; Computed fuel penetration and temperature contours for (d) KH model at 1 ms, (e) KH model at 1.5 ms, (f) KH-ACT model at 1 ms, and (g) KH-ACT model at 1.5 ms after SOI. Solid and dashed white lines indicate flame lift-off length and liquid length, respectively.

and 108 × 108 mm for images in Fig. 11d–g. The flame lift-off location is indicated by the white solid line in these images. Fig 11a shows the flame and its lift-off location as measured by Siebers and Higgins [4], while Fig. 11b and c shows the corresponding flame and lift-off location computed using the KH and KH-ACT model, respectively. A zoomed view of the flame base region is shown to emphasize the flame stabilization location. While the flame shape is well captured by both the models, the flame lift-off length is better predicted by the KH-ACT model. As discussed earlier, the KH-ACT model enhances primary breakup producing smaller droplets, and thus increasing vaporization rate and improving fuel–air mixing. This causes ignition and flame stabilization locations to be closer to the nozzle exit, i.e., it decreases the lift-off length for the KH-ACT model compared to the KH model. The smaller lift-off length predicted by the KH-ACT model is also observed from the comparison of Fig. 11d with f, and of Fig. 11e

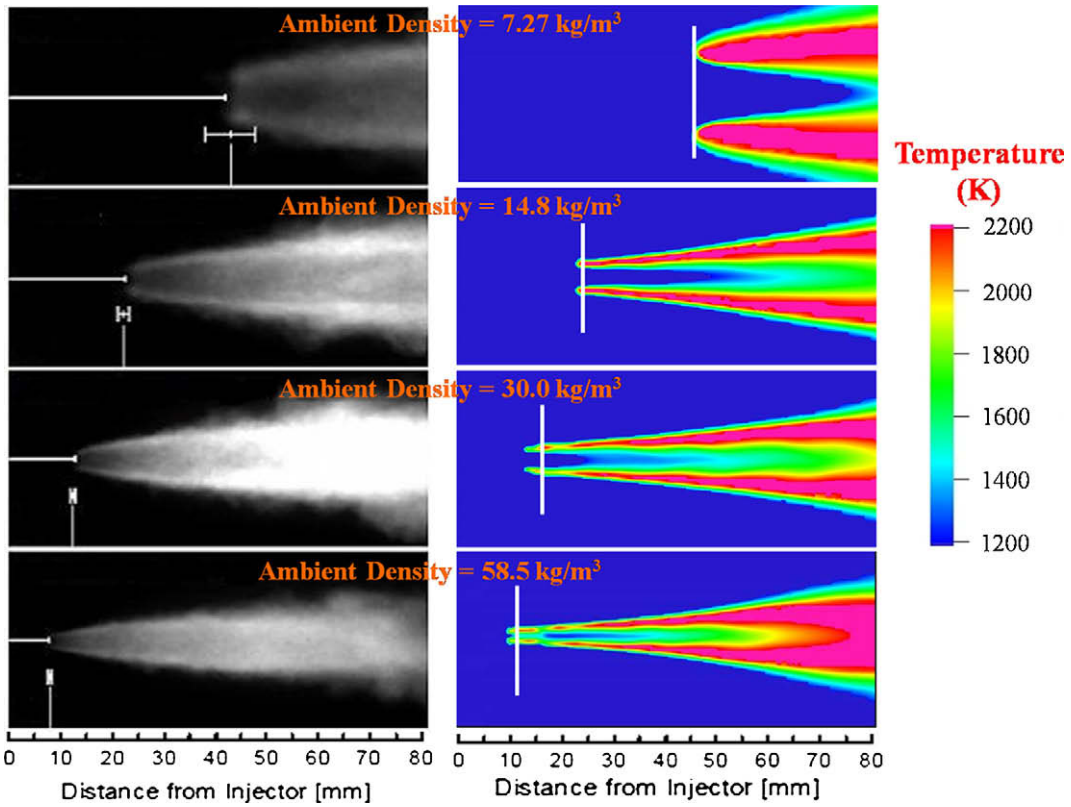

Fig. 12. Comparison of predictions (temperature contours on the right) of the KH-ACT model with measurements (flame images on the left) of Siebers and Higgins [4] at different ambient gas densities. Solid white line in each image indicates flame stabilization location or lift-off length.

with g. Although difficult to see from the images, liquid length also decreases with the KH-ACT model, as expected based on our preceding discussion. An important observation from these images is that the KH-ACT model predicts the liquid length (white dashed lines) to exceed the flame lift-off length, while the KH model predicts otherwise. For these conditions, the measurements also indicated that the liquid length exceeds the flame lift-off length [4,5]. As discussed in the cited study, the interplay between liquid length and lift-off length has important implications for in-cylinder diesel engine processes. For conditions with lift-off length greater than liquid length, fuel vaporization is complete prior to combustion, with minimum interaction between vaporization and combustion processes. However, when lift-off length is shorter than liquid length, there is interaction between vaporization and combustion. Combustion will enhance fuel vaporization thus decreasing the liquid length, while fuel vaporization will decrease the flame temperature causing the flame stabilization location to move downstream, i.e., increasing the lift-off length. Thus the KH model fails to predict a key attribute for this condition investigated, while the KH-ACT model captures this trend accurately.

Fig. 12 presents a comparison of the measured and computed flame images, obtained using KH-ACT model, at different ambient densities. Figs. 13 and 14 present corresponding images at different ambient temperatures and ambient oxygen mole fractions, respectively. Again the flame lift-off location is shown by the white solid line in these images. A good agreement is observed between measured and computed flame images using the KH-ACT model. Thus simulations using the KH-ACT model capture the effects of ambient density, temperature, and oxygen mole fraction on the flame structure fairly accurately. As the ambient density (or ambient pressure) increases, it decreases the injection velocity at the nozzle exit, and consequently decreases both the liquid and vapor lengths. The liquid penetration and liquid length also decrease due to the increased droplet drag caused by higher ambient density. The decrease in liquid and vapor lengths causes the flame stabilization location to move upstream. This behavior is well captured by the simulations, as indicated in Fig. 12. Similarly, the effects of ambient temperature on the flame structure and stabilization are well captured by the simulations, as shown in Fig. 13. An increase in ambient temperature causes two effects. First, it increases the vaporization rate, which decreases the liquid and vapor length, and thus moves the flame stabilization location upstream. Second, it increases the flame reactivity, which also moves the ignition and flame stabilization locations upstream, and thus decreases the flame lift-off length. Fig. 14 shows the effect of ambient oxygen concentration on the flame structure and stabilization location. As the oxygen concentration is reduced, it decreases the flame reactivity (or the Damköhler number) and effectively enhances the EGR effect. As a consequence, the ignition location and the flame base move downstream, increasing the flame lift-off length. Simulations using the KH-ACT breakup model also capture these effects fairly well.

Fig. 15 presents a quantitative comparison between measurements and predictions of the two breakup models, in terms of

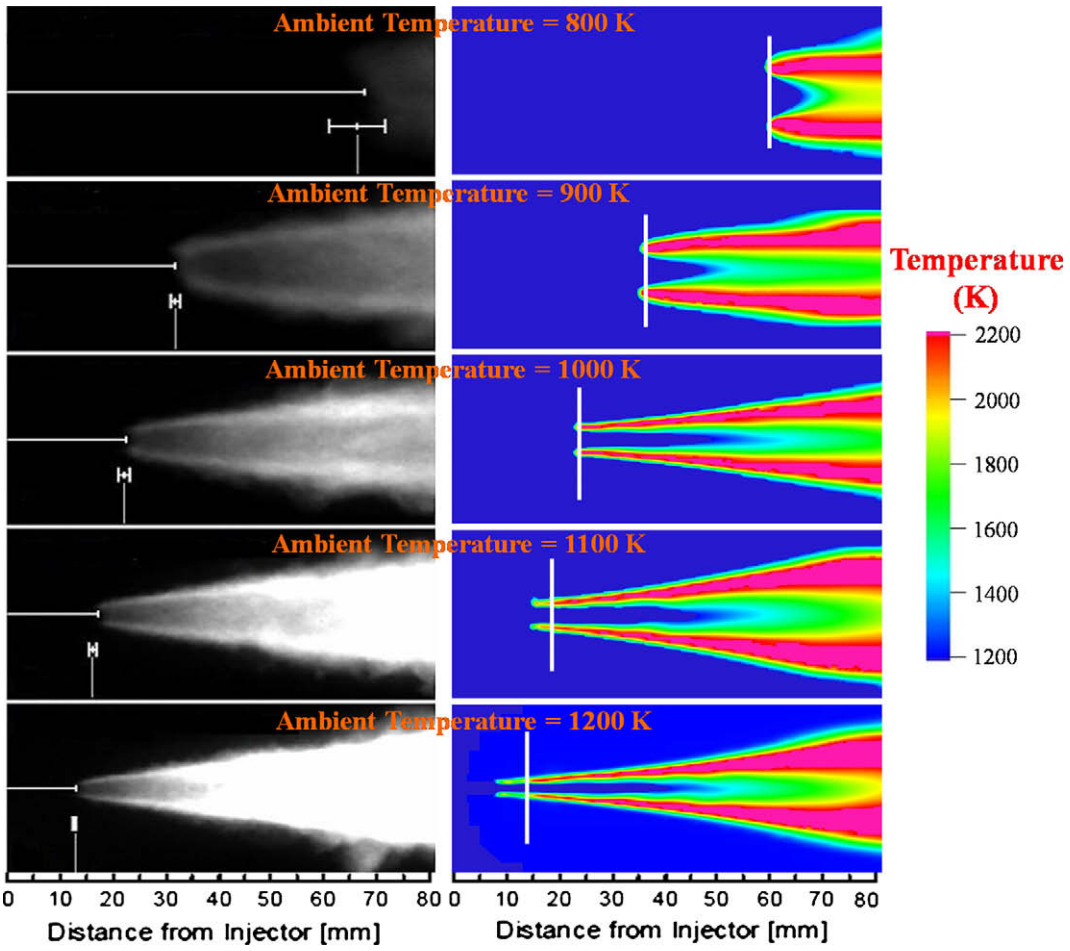

Fig. 13. Comparison of predictions (temperature contours on the right) of the KH-ACT model with measurements (flame images on the left) of Siebers and Higgins [4] at different ambient temperatures. Solid white line in each image indicates flame lift-off length.

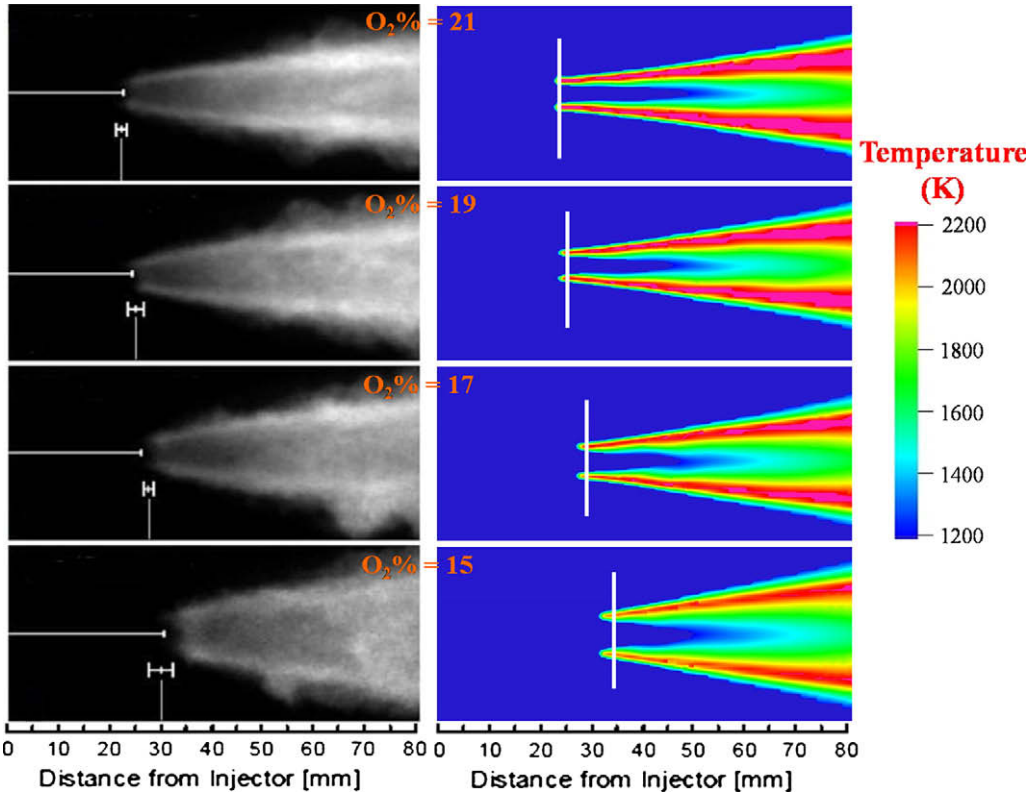

Fig. 14. Comparison of predictions (temperature contours on the right) of the KH-ACT model with measurements (flame images on the left) of Siebers and Higgins [4] at different ambient oxygen mole fractions. Solid white line in each image indicates the flame lift-off length.

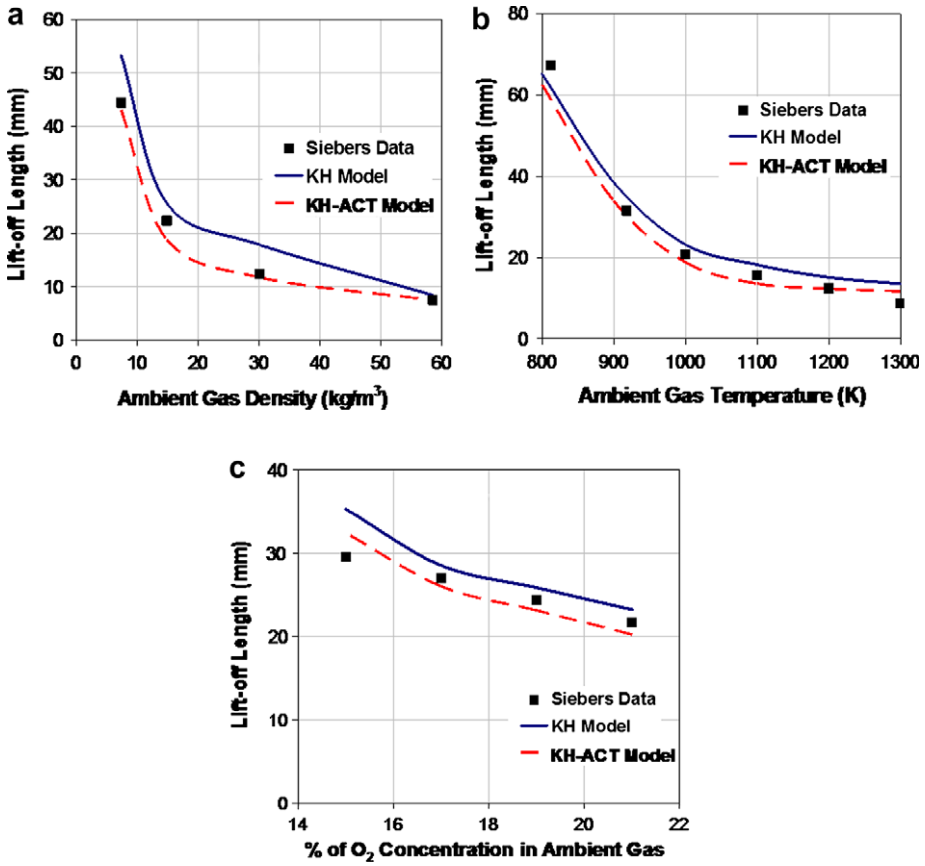

Fig. 15. Comparison of predictions using the KH and KH-ACT models and measurements of Siebers and Higgins [4] in terms of the flame lift-off length vs. (a) ambient gas density, (b) ambient gas temperature, and (c) O_2 mole fraction. Other conditions correspond to the base case (Table 3).

the flame lift-off length plotted vs. the ambient gas density, temperatures and oxygen mole fractions. The lift-off length values correspond to the time at which the flame base becomes stabilized. Both the models capture the qualitative trends reasonably well. However, the KH-ACT model shows better agreement with the experimental data, especially at typical diesel engine conditions, i.e., at higher ambient density and temperatures, and lower O_2 concentrations. Moreover, the lift-off length predicted by the KH-ACT model is lower than that predicted by the KH model. As mentioned earlier, the KH-ACT model enhances primary breakup thus producing smaller droplets and enhancing the vaporization rate, and thus the fuel–air mixing. This causes ignition and flame stabilization locations to be closer to the nozzle exit for this model compared to the KH model.

The last set of results focus on analyzing the lifted flame structure under diesel engine conditions. The diesel engine combustion is typically characterized by two-stage partially premixed flame [45], as illustrated in Fig. 16c, describing the "conceptual model" of Dec [1], based on laser-sheet imaging and optical data. The combustion occurs through a rich premixed flame near the stabilization region, and a non-premixed (or diffusion) flame established further downstream, as indicated in this figure. As the injected liquid fuel atomizes and vaporizes, it entrains hot air leading to fuel air mixing and the occurrence of ignition. Following ignition, the flame develops and is established in a fuel rich region. The combustion process near the leading edge of this flame is characterized by rich premixed combustion, whereby the fuel is partially oxidized to form intermediate products or fuel species, mainly, CO, H_2, and intermediate hydrocarbons such as C_2H_2, which are transported to and consumed in diffusion flame at the jet periphery. Thus the products of rich premixed combustion and surrounding air form the diffusion flame. The rich premixed combustion near the flame leading edge also produces most of the soot. The lift-off length is shorter than the liquid length under these conditions, implying significant interaction between fuel vaporization and combustion processes.

In order to spatially resolve the rich premixed (RPZ) and non-premixed (diffusion) (NPZ) reaction zones, a post-processing tool based on a flame index was developed from the 3-D unsteady simulations. The conventional definition of flame index [46,47] is based on the scalar product of fuel and oxidizer mass fraction gradients. However, since fuel (n-C_7H_{16}) is consumed in the RPZ, such a definition will not be able to resolve the NPZ. Consequently, we replaced fuel by CO species in defining the flame index, since most of CO is produced in the RPZ and then consumed in the NPZ. Then the flame index in the present study is defined as follows:

$$\xi_p = \frac{1}{2}\left(1 + \frac{G_{CO.O_2}}{|G_{CO.O_2}|}\right) \quad \text{with} \quad G_{CO.O_2} = \nabla Y_{CO}.\nabla Y_{O_2} \tag{20}$$

where Y_{CO} and Y_{O_2} denote the CO and O_2 mass fractions, respectively. The two reaction zones are then resolved as follows:

$$\begin{aligned} &\xi_p = 0 \Rightarrow \text{Rich premixed reaction zone} \\ &\xi_p = 1 \Rightarrow \text{Non-premixed reaction zone} \end{aligned} \tag{21}$$

Fig. 16a and b present the resolved flame structure, based on the flame index, computed using the KH model and the KH-ACT model, respectively. It is interesting to note that not only the models capture the two reaction zones, i.e., RPZ and NPZ, in terms of their location and shape; they also reproduce the "conceptual model" depicted in Fig. 16c. There are, however, differences in the predictions of the two models. The KH-ACT model provides better agreement with the measurement and with the conceptual model in that it predicts liquid length greater than the lift-off length. In addition, with the KH-ACT model, the role of the rich premixed combustion is enhanced, while that of the non-premixed combustion is reduced (indicated by the shorter NPZ), compared to

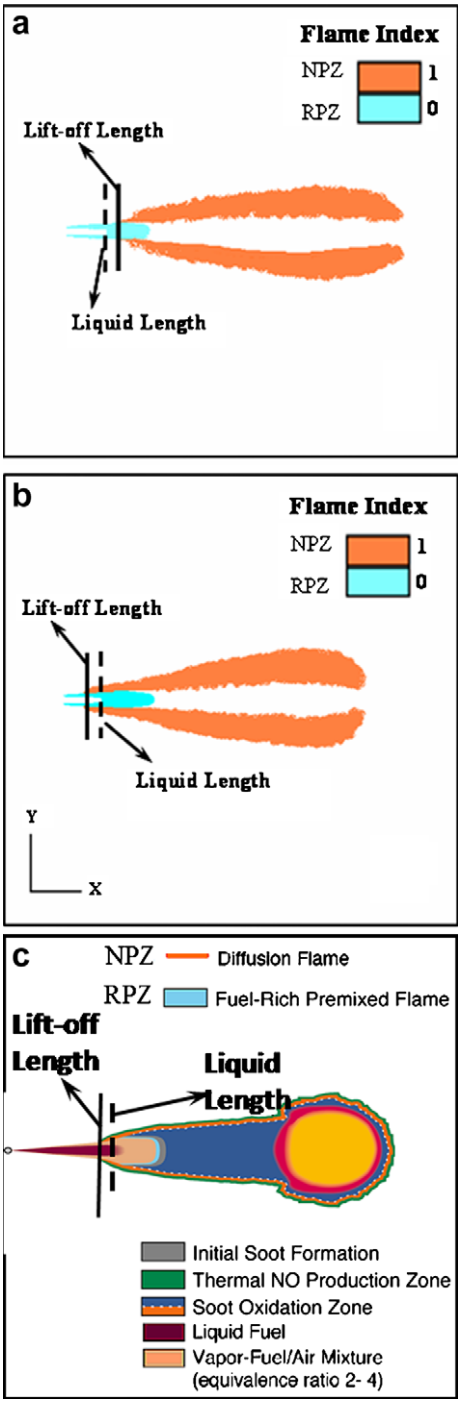

Fig. 16. Comparison of predicted flame structure (in terms of the flame index), using (a) KH model, and (b) KH-ACT model, with the (c) conceptual double-flame combustion model of Dec [1].

that with the KH model. This aspect is further discussed in Fig. 17, which presents the flame structure, computed using the KH and the KH-ACT models, for the base case (with N_2 and O_2 mole fractions being 0.753 and 0.15, respectively). The flame structure is shown in terms of iso-contours of local fuel vapor equivalence ratio and mole fractions of several species (n-C_7H_{16}, O_2, CO, C_2H_2, and OH). These contours clearly depict a partially premixed flame containing the RPZ near the flame stabilization region, and the NPZ around the flame periphery. Thus, the simulations are able to reproduce the "conceptual model" of Dec [1] characterizing diesel

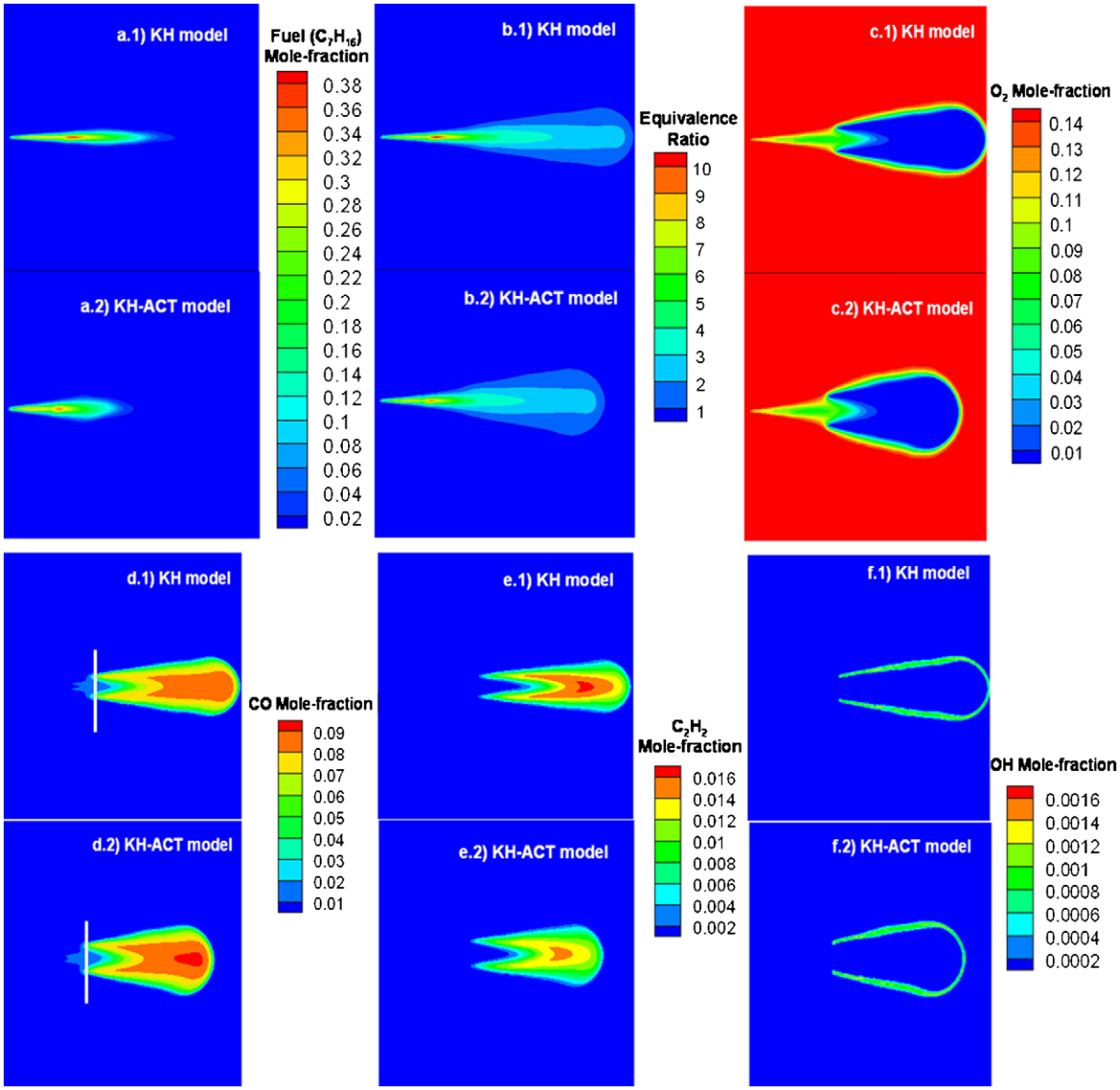

Fig. 17. Comparison of the flame structures computed using the KH model and the KH-ACT models. The flame structure is shown at 2 ms after SOI for the base case in terms of contours of (a) fuel (n-C_7H_{16}) mole fraction, (b) equivalence ratio, (c) O_2, (d) CO, (e) C_2H_2, and (f) OH mole fractions. Solid white lines in (d) indicate the flame lift-off length. The field of view in the axial and radial directions is 108 mm each.

engine combustion. The flame is stabilized in a fuel rich zone, as indicated by the equivalence ratio contours (Fig. 17b). The fuel is completely consumed in the RPZ, producing intermediate fuels such as CO (Fig. 17d), H_2 (not shown here), and C_2H_2 (Fig. 17e). These fuel species are then consumed through a diffusion-controlled combustion process in the NPZ. The OH contours further confirm the double-flame structure, with negligible OH in the RPZ due to rich mixture (equivalence ration exceeding 4.0) in this region. Thus the OH contours locate the diffusion flame region, which is consistent with the observation of Dec [1]. Furthermore, the C_2H_2 and CO contours indicate that most of the soot would be produced in the region downstream of the RPZ, while most of NO_x will be produced in the NPZ, which has the highest temperature (cf. Fig. 16).

Fig. 17 further indicates while both the KH and KH-ACT breakup models are able to reproduce the double-flame structure, there are differences in their predictions. As discussed earlier, the primary breakup process is enhanced with the KH-ACT model, resulting in smaller liquid penetration, smaller droplet size, and greater radial dispersion compared to the KH model. As a consequence, the vaporization and fuel–air mixing are enhanced with the KH-ACT model, which is confirmed by the fuel vapor mole fraction and equivalence ratio contours in Fig. 17. Thus an important difference in the predictions of the two models is that with the KH-ACT model, the flame stabilization point is located further upstream (Fig. 17d), and the role of the rich premixed combustion is enhanced, since the fuel-rich equivalence ratio is reduced (Fig. 17b), while that of the non-premixed combustion is relatively reduced. This is further indicated by the lower C_2H_2 concentrations predicted with the KH-ACT model, and by the O_2 contours (Fig. 17c) and OH contours (Fig. 17f), which indicate a smaller NPZ with the KH-ACT model. These results imply that the predictions of soot and NO_x emissions would also be influenced by the new (KH-ACT) primary breakup model. This aspect will be examined in a future study.

6. Conclusions

We have investigated the effects of primary breakup modeling on the spray and combustion characteristics under diesel engine conditions. Two primary breakup models are examined. The first one considers the aerodynamically induced breakup based on the Kelvin–Helmholtz (KH) instability, while the second (KH-ACT) model includes the effects of cavitation and turbulence, in addition to the aerodynamic effect. These two models are extensively evaluated using measurements for non-evaporating and evaporating sprays, as well as flame measurements under diesel engine conditions. Important observations are:

(1) The inclusion of cavitation and turbulence enhances the primary breakup process, causing smaller droplet sizes, decrease in liquid penetration, and increase in radial dispersion. As a consequence, the KH-ACT model provides closer agreement with the X-ray data for non-evaporating sprays in terms of liquid penetration, spray cone angle and axial velocity, and liquid mass distribution.
(2) For evaporating sprays, predictions using the KH-ACT model exhibit better agreement with measurements with respect to the liquid length and vapor penetration distance for a range of parameters, including injection pressure, fuel temperature, ambient density and temperature. This is again due to the enhanced breakup process predicted with the KH-ACT model. However, the effect of primary breakup model on the predicted spray behavior is less pronounced for evaporating sprays compared to that for non-evaporating sprays.
(3) The enhanced spray breakup modifies fuel–air mixing, and thus influences ignition and combustion characteristics in that the ignition and flame stabilization occur closer to the nozzle exit. As a consequence, the flame lift-off length predicted using the KH-ACT model shows better agreement with measurements for a wide range of diesel engine conditions.
(4) The detailed flame structure indicates that combustion under diesel engine conditions occurs through a rich premixed flame near the stabilization region, and a non-premixed (or diffusion) flame established further downstream. This double-flame structure is consistent with the "conceptual model" of Dec [1] for diesel engine combustion.
(5) A flame index based on the scalar product of CO and O_2 mass fraction gradients was developed for the first time to analyze diesel combustion. The double-flame structure was further confirmed by this flame index.

Acknowledgment

This work has been supported by the US Department of Energy Office of Vehicle Technology under the management of Mr. Gurpreet Singh. Many useful discussions with Anita Ramirez at UIC, and Douglas Longman, Christopher Powell, Alan Kastengren, Stephen Ciatti, and Essam El-Hannouny at Argonne National Laboratory are greatly appreciated.

References

[1] J.E. Dec, SAE Paper 970873, 1997.
[2] P.F. Flynn, R.P. Durrett, G.L. Hunter, A.O. Loye, O.C. Akinyemi, J.E. Dec, C.K. Westbrook, SAE Paper 1999-01-0509, 1999.
[3] J.D. Naber, D.L. Siebers, SAE Paper 960034, 1996.
[4] D.L. Siebers, B. Higgins, SAE Paper No. 2001-01-0530, 2001.
[5] B. Higgins, D.L. Siebers, SAE Paper No. 2001-01-0918, 2001.
[6] D.L. Siebers, SAE Paper 980809, 1998.
[7] D.A. Nehmer, R.D. Reitz, SAE Paper 940668, 1994.
[8] C. Arcoumanis, M. Gavaises, Atomization Sprays 8 (1998) 307–347.
[9] M.A. Patterson, R.D. Reitz, SAE Technical Paper 980131, 1998.
[10] C.Y. Choi, R.D. Reitz, Combust. Sci. Technol. 159 (2000) 169–198.
[11] Y. Yi, R.D. Reitz, SAE Paper No. 01-1041, 2003.
[12] C. Arcoumanis, M. Gavaises, SAE Paper 970799, 1997.
[13] A.A. Amsden, P.J. O"Rourke, T.D. Butler, KIVA-II: A Computer Program for Chemically Reactive Flows with Sprays, Los Alamos National Laboratory Report No. LA-11560-MS, 1989.
[14] N. Abani, S. Kokjohn, S.W. Park, M. Bergin, A. Munnannur, W. Ning, Y. Sun, R.D. Reitz, SAE Paper No. 2008-01-0970, 2008.
[15] G. Blokkeel, B. Barbeau, R. Borghi, SAE Paper No. 2003-01-0005, 2003.
[16] A. Vallet, A.A. Burluka, R. Borghi, Atomization Sprays 11 (2001) 619–642.
[17] J. Benajes, J.V. Pastor, R. Payri, A.H. Plazas, ASME J. Fluid Eng. 126 (2004) 63–71.
[18] R. Payri, F.J. Salvador, J. Gimeno, L.D. Zapata, Fuel 87 (2008) 1165–1176.
[19] R.D. Reitz, F.V. Bracco, Phys. Fluids 25 (1982) 1730–1741.
[20] R.D. Reitz, Atomization Spray Technol. 3 (1987) 309–337.
[21] J.C. Beale, R.D. Reitz, Atomization Sprays 9 (1999) 623–650.
[22] A.H. Lefebvre, Atomization and Sprays, Hemisphere Publishing Corporation, USA, 1989.
[23] S. Som, A.I. Ramírez, S.K. Aggarwal, A.L. Kastengren, E.M. El-Hannouny, D.E. Longman, C.F. Powell, SAE Paper No. 2009-01-0838.
[24] S. Som, S.K. Aggarwal, 47th AIAA Aerospace Sciences Meeting, AIAA-2009-0666, 2009.
[25] P.K. Senecal, E. Pomraning, K.J. Richards, T.E. Briggs, C.Y. Choi, R.M. McDavid, M.A. Patterson, SAE Paper No. 2003-01-1043, 2003.
[26] P.K. Senecal, E. Pomraning, K.J. Richards, T. Yang, M.Z. Dai, R.M. McDavid, M.A. Patterson, S. Hou, T. Shethaji, SAE Paper 2007-01-0159, 2007.
[27] K.J. Richards, P.K. Senecal, E. Pomraning, CONVERGE™ (Version 1.2) Manual, Convergent Science Inc., 2008.
[28] Som S. Development and Validation of Spray Models for Investigating Diesel Engine Combustion and Emissions. PhD Thesis, University of Illinois at Chicago; 2009.
[29] K.Y. Huh, A.D. Gosman, in: Proceedings of the international conference of multi-phase flows, 1991, pp. 515–518.
[30] G.M. Bianchi, P. Pelloni, F.E. Corcione, L. Alloca, F. Luppino, J. Eng. Gas Turb. Power 123 (2001) 419–427.
[31] E.V. Berg, W. Edelbauer, A. Alajbegovic, R. Tatschl, M. Volmajer, B. Kegl, L.C. Ganippa, ASME J. Eng. Gas Turb. Power 127 (2005) 897–908.
[32] D.P. Schmidt, C.J. Rutland, J. Comput. Phys. 164 (2000) 62–80.
[33] S.L. Post, J. Abraham, Int. J. Multiphase Flow 28 (2002) 997–1019.
[34] A.B. Liu, D.K. Mather, R.D. Reitz, SAE paper No. 930072, 1993.
[35] <http://www.tfd.chalmers.se/~valeri/MECH.html>.
[36] S. Som, S.K. Aggarwal, ASME Paper IMECE2008-68441.
[37] S. Som, S.K. Aggarwal, E.M. El-Hannouny, D.E. Longman, ASME J. Eng. Gas Turb. Power 132 (4) (2010) 1–12.
[38] E.C. Brennen, Cavitation and Bubble Dynamics, Oxford University Press, 1995.
[39] A.I. Ramirez, S. Som, S.K. Aggarwal, A.L. Kastengren, E.M. El-Hannouny, D.E. Longman, C.F. Powell, Exp. Fluids 47 (2009) 119–134.
[40] A.I. Ramírez, S. Som, S.K. Aggarwal, A.L. Kastengren, E.M. El-Hannouny, D.E. Longman, C.F. Powell, 21st ILASS Americas, 2008.
[41] S. Som, S.K. Aggarwal, Atomization Sprays 19 (9) (2009) 885–903.
[42] H. Chaves, C. Kirmse, F. Obermeier, Atomization Sprays 14 (2004) 589–609.
[43] S. Wissel, G. Grünefeld, Appl. Phys. B: Lasers and Opt. 83 (2006) 181–184.
[44] A.L. Kastengren, C.F. Powell, T. Reidel, S.K. Cheong, K.S. Im, X. Liu, Y. Wang, J. Wang, J. Fluid Eng. 130 (2008) 041301-1–12.
[45] Z. Shu, B.J. Krass, C.W. Choi, S.K. Aggarwal, V.R. Katta, I.K. Puri, Proc. Combust. Inst. 27 (1999) 625–632.
[46] H. Yamashita, M. Shimada, T. Takeno, Proc. Combust. Inst. 26 (1996) 27–34.
[47] A.J. Lock, A.M. Briones, X. Qin, S.K. Aggarwal, I.K. Puri, H. Hegde, Combust. Flame 143 (2005) 159–173.